

# Oxygen mass transfer and shear stress effects on *Pseudomonas putida* BCRC 14365 growth to improve bioreactor design and performance

Hamed Moradkhani<sup>1</sup> · Mir-Shahabeddin Izadkhah<sup>2</sup> · Navideh Anarjan<sup>3</sup> · Abolfazl Abdi<sup>2</sup>

Received: 19 May 2017 / Accepted: 24 July 2017 / Published online: 12 August 2017  
© Springer-Verlag GmbH Germany 2017

**Abstract** In this work, the experimental evidence is presented for two basic issues including oxygen mass transfer and shear analysis on the microorganism containing medium on the most prominent sections of the bioreactor. Computational fluid dynamics (CFD) methodology reproduces shear rate values for specific impeller designs using the commercial code (Fluent 6.2). CFD calculates volumetric mass transfer coefficient based on the Higbie's penetration theory. Four types of impeller are used. The spherical probe is used to measure flow hydrodynamic parameters to obtain shear rate by electro-diffusion (ED) method. The obtained results are validated experimentally and it is shown that a fully axial pattern impeller represents more enhanced results than partially axial and radial. In this regard, experimental results for volumetric oxygen mass transfer coefficient ( $k_L a$ ) confirm CFD predictions by

acceptable deviations of 2.65, 8.90, and 9.20 for 0.15, 0.2, and 0.3 VVM, respectively. These results collaboratively indicate that LIGHTNIN–C 200 type operates more efficiently by reflecting the flow to the bottom corner stagnation areas with the minimum tolerable shear and the most velocity distribution uniformity. Furthermore, the values of  $k_L a$  improve by aeration rate. Conversely, increasing the rotational speed of impeller creates difficulties for cell growth due to the generated harsh shear condition. CFD provide a better understanding of how operational and geometrical variables may be manipulated to achieve a moderate shear rate and acceptable level of mass transfer.

**Keywords** Shear rate · Microorganism · Electro-diffusion method · Experimental · CFD · Mass transfer

---

Responsible editor: Gerald Thouand

✉ Hamed Moradkhani  
Hamed.moradkhani@yahoo.com

<sup>1</sup> Environmental Engineering Research Center (EERC), Faculty of Chemical Engineering, Sahand University of Technology, P.O. Box 513551996, Sahand New Town, Tabriz, Iran

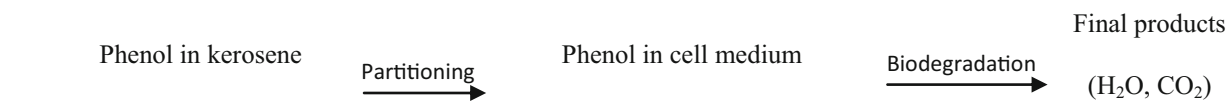
<sup>2</sup> Department of Chemical and Petroleum Engineering, University of Tabriz, P.O. Box 5166616471, Tabriz, Iran

<sup>3</sup> Department of Chemical Engineering, Tabriz Branch, Islamic Azad University, P.O. Box 5157944533, Tabriz, Iran

## Introduction

The presence of phenol as a typical toxic contaminant in many industrial wastewaters at lower concentration levels adds an unpleasant taste to drinking water (Juang et al. 2012). These organic pollutants are being degraded even at lower concentrations in the bioreactors by microorganisms (Juang et al. 2012). Biodegradation by microorganisms is a promising environmentally friendly alternative for the costly and inefficient physical and chemical methods in terms of removing pollutants from water resources. The process of phenol partitioning from the

organic phase into the cell medium for biodegradation has the following steps:



Oxygen aerated to the medium for the growth and metabolic activity of microorganisms is a key substrate in most of the microbial oxidative bioconversions in industry (Moutafchieva et al. 2013; Sungkorn et al. 2012; Zokaei-Kadijani et al. 2013). Biodegradation takes place in a multi-phase system including gas phase and two immiscible liquid phases (Melgarejo-Torres et al. 2011). The aqueous phase culture containing microorganisms and mineral salts extracts pollutant substances at low levels from the organic solvent, which is the concept of the two-phase partitioning bioreactors (TPPBs). The idea of TPPB is first proposed by Daugulis and Collins for the case of phenol degradation by *Pseudomonas putida* strain in 1996.

Oxygen mass transfer is a function of many variables such as the geometry of the impeller and operational conditions (Labik et al. 2017; Puthli et al. 2005; Scargiali et al. 2014; Trad et al. 2017). Therefore, mass transfer is sufficiently affected by the type and speed of impeller in addition to the gas flow rate used (Gogate and Pandit 1999). Efficient gas distribution and higher residence time for oxygen bubbles in the cell medium are achievable by excellent mixing, which is in direct correlation with the appropriate selection of impeller design in bioreactors. Prediction of oxygen mass transfer coefficient is of vital importance, as it is a limitation for bioreaction kinetics owing to the low solubility of oxygen. Studying various operational and geometrical parameters of bioreactors is essential to make suggestions for better gas-liquid mass transfer (Puthli et al. 2005). Oxygen solubilization and diffusion rates into the target medium and nutrient transfer to maintain cells in suspension are expressed in terms of volumetric mass transfer coefficient ( $k_L a$ ) that comprises the liquid-side mass transfer coefficient ( $k_L$ ) and specific gas-liquid mass transfer area ( $a$ ) (Moutafchieva et al. 2013). CFD capability to predict local  $k_L a$  values would be valuable for making suitable decisions for impeller selection and more robust scale-up and design purposes.

Microorganisms cannot generally survive in organic medium with severe conditions. This issue is often referred to as bioavailability (Juang et al. 2010; Juang et al. 2012). In biochemical processes, shear rate is not important by itself; however, interfacial shear rate affects system efficiency due to its adverse impact on biomass concentration. Excessive shear is known to damage suspended cells, which lead to the loss of viability and even disruption (Wase et al. 1985). Therefore, minimum agitation speed is preferred, especially in the

impeller region, for inherently stress-sensitive microorganisms (Laurenzi et al. 2009). *P. putida* is a stress-sensitive filamentous phenotype in response to environmental stress conditions during its natural life cycle. The aerobic rod-shape bacterium is sensitive to filament-inducing conditions (Malleve et al. 2016). *P. putida* strain is selected as a bacterial model which is able to degrade a wide range of organic chemicals, making it a good candidate for environmental engineering studies. The study of mixing key parameters mainly agitation along with aeration due to their impacts on the procurement of oxygen for microorganisms during bioprocesses has attracted the attention of researchers (Dey et al. 2016; Zhao et al. 2017). According to many studies about the mechanical damages of freely suspended cells, agitation and aeration are two main causes of shear-sensitive cell death which takes place by bursting bubbles at the air-liquid interface (Scargiali et al. 2014). Consequently, bioreactors have to be designed according to the shear tolerance of biological systems, which means the acceptable level of shear rates that provide a gentle culture environment (Contreras et al. 1999). Therefore, in addition to  $k_L a$  value, the performance and behavior of bioreactors can be estimated by shear rate analysis in different geometrical and operational conditions calculated by velocity gradients. The dynamic mechanical behavior of a single biological cell can be investigated by mechanical methods such as micro-fluid and shear stress devices (Kohles et al. 2009). This can lead to large localized forces of shear to the cell wall surfaces resulting in cell rupture (Doulah 1977). Doulah et al. (1975 and then Doulah (1977) have described the theory of shear stress as a primary cause of microorganism rupturing. Wilson and Kohles (2010) identified in their recent simulation research a range of potential mechanical strains that can be produced in multi-axial fluid-induced stress.

CFD techniques use numerical solutions of flow transport conservation equations to cover a wide range of conditions going on in industrial units to achieve acceptable predictions. CFD has proved to be affordable for modeling of complex multiphase bioreactions taking place in stirred vessels with inherent complicated configurations (Moradkhani et al. 2016).

In the present study, a variety of impeller selections based on shear rate experimental measurements is considered by the electro-diffusion technique. Data obtained from the study of various impellers could be used for confirming the CFD shear analysis in the mixing

bioreactor. CFD simulation could be helpful to obtain velocity gradient in order to calculate shear values in different positions of bioreactor. These results could be used to identify locations where the probability of microorganism rupture is the most. After a comprehensive literature review, it is essential to mention that it has been less discussed about the application of CFD in shear analyzing of microorganisms in the literature and should be further much focused on. As a novelty feature, the comparative study of oxygen mass transfer issue besides shear sensitivity in different operational and geometrical conditions of aerobic bioreactor designs has been conducted. As a result of this approach, the survival conditions of organisms can be considered in process modeling and optimization.

## Materials and methods

### Experimental

In order to respond to the validation recognizance of the work, experimental measurement of the shear rate was performed to come along with CFD model.

#### *Shear rate determination by electro-diffusion measurement method*

The velocity field in the boundary layers of moving solid objects in bioreactors can hardly be investigated by common visualization tools such as particle image velocimetry (PIV) method to get linked with shear rate. Direct measurement of shear stress is a difficult task due to the sensitivity limitations of sensors. One of the well-known techniques for wall shear measurements is the current limitation electro-diffusion method, which can be used for moving parts as well as the stationary. In this method, mass transfer is employed to calculate the hydrodynamic parameters of the flow, which means that wall shear rate over the surface boundary of the probe is calculated using the local diffusion limiting current,  $I_d$ , resulting from the fast reduction of ferricyanide ions. On the account of sturdiness, this technique can be applied for measurement in high viscosity aerated stirred bioreactors. Because of high turbulent intensities in such bioreactors, the flow parameters must be detected in each direction (Franz et al. 1984; Menzel et al. 1985). The probe types described in the literature could report the sign and magnitude of one component of shear rate vector. These probes are restricted to one directional flows such as pipe flows. However, there are other types of probes that are able to determine absolute values of shear rate regardless of flow direction (Pauli et al. 1989). In the current study, the spherical probe is used to measure flow hydrodynamic required parameters and obtain shear rate by interrelation

to the measured data according to the following equation (Pauli et al. 1989):

$$\gamma = \left( \frac{1.477}{n_z F} \right)^3 \cdot \frac{I_d^3}{D_{eff}^2 C_0^2 d_e^5} \tag{1}$$

where  $D_{eff}$  is the molecular diffusivity of ferric ions in the solution,  $n$  denotes the number of transferred electrons,  $F$  is the Faraday constant (96,485.3329 s A/mol),  $C_0$  is the concentration of reacting component,  $I_d$  is the sum of currents, and  $d_e$  represents the electrode diameter.

#### *Microorganism and nutrient medium*

*P. putida* Bioresource Collection Research Center (BCRC) 14365 was obtained from Food Industry Research and Development Institute, Hsinchu, Taiwan. The microorganisms were stored at 4 °C. The bacteria grew on a mineral medium prepared with deionized water with phenol as the sole carbon and energy source (Table 1).

**Free microorganism cultivation process** Phenol of 100 g/m<sup>3</sup> was added to the mineral medium containing activated *P. putida* cells for adaptation at 30 °C for 24 h. The cells were collected after centrifugation and re-suspended in the phosphate buffer. The activated cells were cleaned by centrifugation and inoculated into the culture medium to give the initial concentration of 57 g/m<sup>3</sup>, corresponding to the optical density of 0.120 at 600 nm. The number of colonies was determined by the serial dilution of the culture, and 0.15 cm<sup>3</sup> of the diluted culture was spread on a plate. The plate was then incubated overnight at 30 °C. Afterwards, the number of colonies was counted.

#### *Experimental determination of oxygen mass transfer coefficient ( $k_L a$ )*

The experimental set-up, as depicted in Fig. 1, was according to the experimental work by Juang et al. (2010). Dimensions of the bioreactor used for the removal of phenol are illustrated in Fig. 2. A dissolved oxygen electrode (Extech, DO600-k, USA) was installed in different positions of the reactor (Fig. 3). The volumetric oxygen transfer coefficient ( $k_L a$ ) was obtained by continuous gassing-out procedure (Ferreira et al. 2012; Michelin et al. 2013). The transient variations of the inlet oxygen concentration resulted in the time-dependent consequences of dissolved oxygen concentration in the cell culture medium. These incremental changes were used to calculate the mass transfer coefficient according to the following equation (Ramezani et al. 2015):

$$\ln(C^* - C_L) = \ln(C^* - C_0) - k_L a \cdot t \tag{2}$$

**Table 1** Composition of the synthetic medium

Phase	Components	Concentration (g/m <sup>3</sup> )	Phase volume fraction	Phase viscosity (kg/m.s)	Phase density (kg/m <sup>3</sup> )
Aqueous	Water	Solvent	0.66	0.0016	162
	Microorganism	57			
	Phenol	300			
	KH <sub>2</sub> PO <sub>4</sub>	420			
	K <sub>2</sub> HPO <sub>4</sub>	375			
	(NH <sub>4</sub> ) <sub>2</sub> SO <sub>4</sub>	244			
	NaCl	15			
	CaCl <sub>2</sub> ·2H <sub>2</sub> O	15			
	MgSO <sub>4</sub> ·7H <sub>2</sub> O	50			
	FeCl <sub>3</sub> ·6H <sub>2</sub> O	54			
Organic	Kerosene	Solvent	0.34	0.0008	950.11
	Phenol	910.11			

In the case, where  $C_0 = 0$ :

$$\ln\left(\frac{C^* - C_L}{C^*}\right) = -k_L a t \quad (3)$$

where  $C^*$  is the saturation concentration of oxygen (7.33 g/m<sup>3</sup>) and  $C_L$  is the local oxygen concentration. The volumetric mass transfer coefficient was determined by the variation of  $\ln(C^* - C_L)$  value against time (t).

## Development of CFD simulation

### Eulerian model

This research applied the Eulerian multi-fluid method to predict the behavior of the gas and liquid interactions in an aerobic biodegradation system. In this paper, data from the very basic and standard CFD simulation of a number of single impellers operated in a small-scale gas-liquid mixing vessel were presented. A significant assumption in the CFD is that the bubble size is spatially uniform, whereas we know from the experiments that the bubble size distribution is slightly heterogeneous in small-scale bioreactors. Therefore, CFD method with average bubble size distribution is suitable if we overlook to explore the change of bubble volume in the up-moving process. On the other side, this phenomenon of bubble size changes is rather important and significant only in large-scale bioreactors. According to this model, the Eulerian governing equations of fluid motion are separately solved for each phase (Fluent 2006). The continuity equation for phase  $i$  is as follows:

$$\frac{\partial}{\partial t}(\alpha_i \rho_i) + \nabla \cdot (\alpha_i \rho_i U_i) = 0 \quad (4)$$

where  $\alpha_i$ ,  $\rho_i$ , and  $U_i$  represent the volume fraction, density, and Reynolds-averaged velocity, respectively.

$$\sum_{i=1}^2 \alpha_i = 1 \quad (5)$$

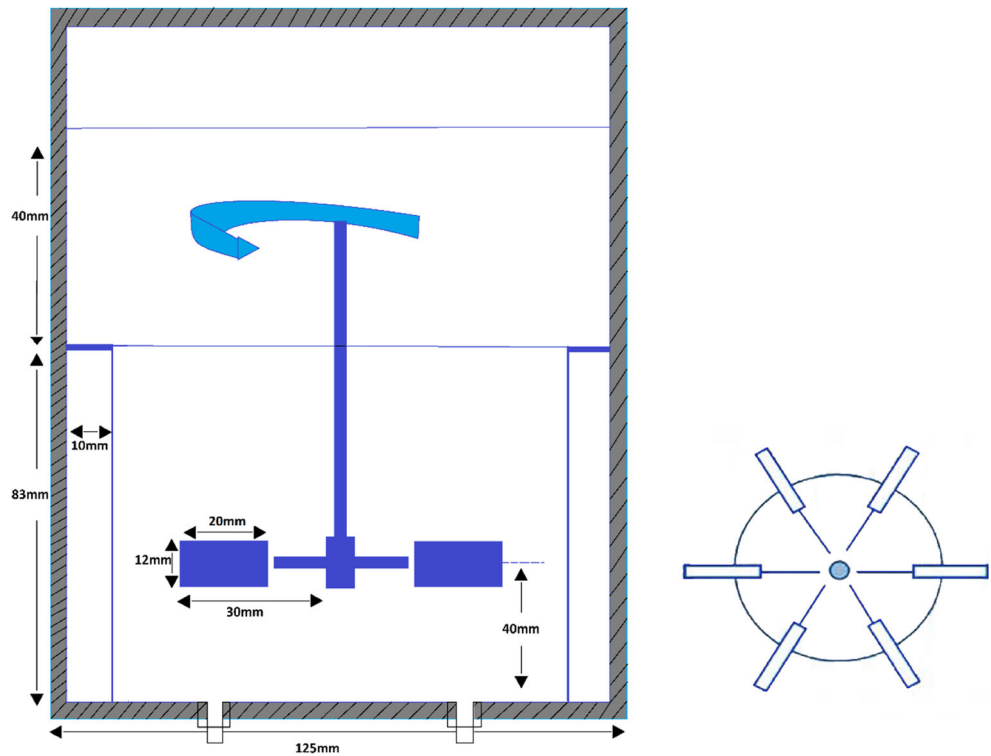
The momentum conservation equation in the time-averaged form for each phase yields (Anderson and Wendt 1995):

$$\begin{aligned} \frac{\partial}{\partial t}(\alpha_i \rho_i U_i) + \nabla \cdot (\alpha_i \rho_i U_i U_i) = & -\alpha_i \nabla P_i + \alpha_i \rho_i g \\ & + \nabla \cdot (\alpha_i \bar{\tau}_{eff}) + F_i \\ & + F_{c_i} \end{aligned} \quad (6)$$



**Fig. 1** Experimental set-up: lagged bioreactor (a). DO meter electrode (b). Spherical probe for electro-diffusion method (c)

**Fig. 2** Dimensions of the bioreactor used for removal of phenol



where  $\tau_{eff}$  is the effective viscous stress tensor considering the turbulent effects related to the mean velocity gradient and  $\tau_i$  is the  $i^{th}$  phase stress-strain tensor.

$$\tau_{lam,i} = \mu_i [\nabla U_i + (\nabla U_i)^T] + \lambda (\nabla \cdot U_i) I \tag{7}$$

$$\tau_{tur,i} = \mu_{tur,i} \left[ \left[ \nabla U_i + (\nabla U_i)^T \right] - \frac{2}{3} (\nabla \cdot U_i) I \right] - \omega \rho_i k_i I \tag{8}$$

The parameter  $\lambda$  is defined as

$$\lambda = -\frac{2}{3} \mu_i \tag{9}$$

and  $k_i$  is the turbulent kinetic energy for phase  $i$ . The terms  $\tau_{lam}$  and  $\tau_{tur}$  are the laminar and turbulent viscous shear stress terms in the momentum equation, respectively. In addition,  $T$  is the superscript in the form of tensor to indicate the transpose of  $\nabla \cdot U$ . The parameter  $\omega$  is equal to  $2/3$  for the continuous phase whereas its value for dispersed phases depends on their volume fractions (Ahmadi and Ma 1990).

The term  $\tau_{eff}$  is the effective molecular viscosity, which is the summation of the viscosity and turbulent viscosity of each phase.

$$\bar{\tau}_{eff} = \tau_{tur,i} + \tau_{lam,i} \tag{10}$$

The effective viscous stress tensor is determined by the following equation (Anderson and Wendt 1995):

$$\bar{\tau}_{eff} = (\mu_{lam,i} + \mu_{tur,i}) (\nabla U_i + \nabla U_i^T) - \frac{2}{3} \left( \frac{3}{2} \omega \rho_i k_i + (\mu_{lam,i} + \mu_{tur,i}) \nabla \cdot U_i \right) I \tag{11}$$

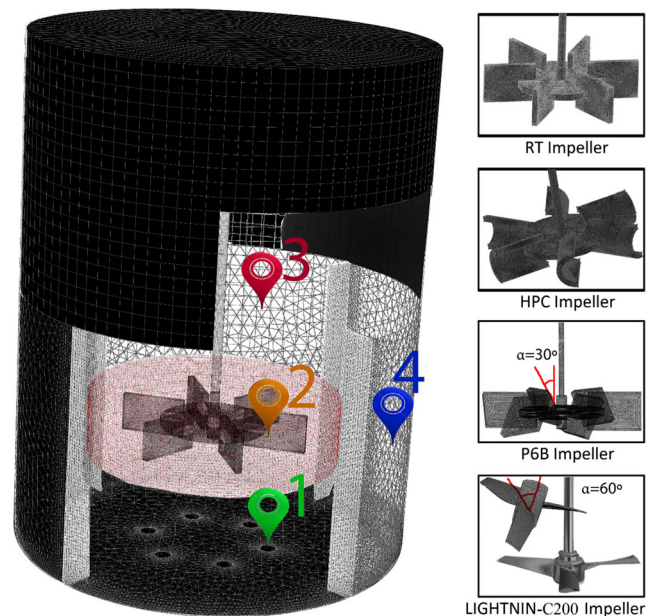


**Fig. 3** Bioreactor and impeller configuration and computational grid

The term  $F_{i_i}$  in Eq. (6) is the interphase force acting on phase  $i$  due to the presence of the other phases. The term  $F_c$  represents centrifugal forces applied to the impeller region in the rotating reference frame for the multiple reference frame (MRF) model.

In the stationary frame:

$$\vec{F}_{c_i} = 0 \quad (12)$$

In the rotating frame:

$$\vec{F}_{c_i} = -2\alpha_i\rho_i\vec{N} \times \vec{U}_i - \alpha_i\rho_i\vec{N} \times (\vec{N} \times \vec{r}) \quad (13)$$

where  $N$  is the number of rotations around the impeller axis in 1 min.

MRF solves the equations of motion in both stationary (for absolute velocity) and rotating (velocity in the rotating reference) frames.

Among the interphase momentum exchange source terms of the participant forces, drag force plays the most influential and controlling role, since it is predominant over the lift and virtual mass. The interphase force can mainly be expressed by Ishii and Zuber (1979) model:

$$F_{ii} = \sum F_{i-j} \\ = \left(\frac{3}{4}\right) \left( \sum_j^N \frac{C_{D,i-j}}{d_i} \rho_i \alpha_j |U_j - U_i| (U_j - U_i) \right) \quad (14)$$

The subscript  $j$  in Eq. (14) denotes the dispersed phase number. The drag coefficients are obtained by the standard correlation of Schiller and Neumann for the spherical bubbles and organic phase droplets with diameter of  $d_j$  (Bartrand et al. 2009; Qi et al. 2013).

$$\begin{cases} C_{D,i-j} = \max\left(\frac{24}{Re} (1 + 0.15Re^{0.687}), 0.44\right) \\ Re = \frac{\rho_i d_j |U_j - U_i|}{\mu_i + C\mu_{t,i}} \end{cases} \quad (15)$$

where  $C$  stands for the model parameter introduced to account for the effect of the turbulence in reducing slip velocity (Bakker and Akker 1994). Bakker recommended the value of 0.02 for  $C$  which depends on the hydrodynamic of stirred gas-liquid dispersions (Bakker 1992). The “pressure outlet” boundary condition was specified for the atmospheric pressure above the liquid surface level for the gas phase. Furthermore, for the liquid phases, no-slip boundary condition is defined for the solid moving walls, namely the shaft and impeller blades and in the same way for the stationary walls of the baffles and the rest parts of the vessel. Similarly, free-slip condition is selected for the gas bubbles. The value of gravitational acceleration vector in negative  $Z$

direction is  $9.81 \text{ m/s}^2$ . Different gas flow rates with volume fraction equal to unity and with defined axial rise velocity of gas bubbles are defined as the velocity inlet boundary condition at orifice surfaces (mark 1 in Fig. 3), whereas the normal liquid rise velocity is given zero. Turbulent intensity at gas inlet is set to moderate value of 15% in turbulence boundary conditions.

#### Shear rate calculation

The characteristic value for the shear rate, the modulus of the rate of strain tensor, is according to the following definition (Anderson and Wendt 1995):

$$\gamma = \left( \frac{\partial U_i}{\partial x_j} + \frac{\partial U_j}{\partial x_i} \right) \quad (16)$$

Friction is determined as:

$$\tau_{ij} = -\mu_{tur}\gamma_{ij} \quad (17)$$

Turbulent shear flow is a modification of completely homogeneous flow to allow for shear stresses and for well-defined mean velocity gradients, such as those found in a jet, a mixing layer, or a boundary layer. One or two of the Reynolds shearing stresses are usually zero (Paul et al. 2004).

#### Oxygen mass transfer model

Mass transfer coefficient  $k_L$  in bioreactors can be estimated by theoretically based models. According to the Higbie’s penetration theory which is proposed to predict the mass transfer coefficient, there are some resistance to oxygen transfer for small molecules with diffusion coefficient in the gas phase much greater than in the liquid phase and with very low solubility in the most liquid phases. The value of  $k_L$  depends on the distribution of the energy dissipation from viscous mixing. Consequently, oxygen mass transfer depends on the local value of,  $\varepsilon$ , the kinetic energy dissipation rate.

The mass transfer coefficient for gas-liquid penetration is calculated by the following correlation used by Lamont and Scott (Kawase et al. 1992; Laakkonen et al. 2007; Lamont and Scott 1970):

$$K_L = \frac{2}{\sqrt{\pi}} D^{0.5} \left( \frac{\varepsilon_{aqs} \rho_{aqs}}{\mu_{aqs}} \right)^{0.25} \quad (18)$$

where  $D$  is the diffusion coefficient which has been evaluated from the Wilke-Chang correlation ( $1.78 \times 10^{-5} \text{ m}^2/\text{s}$ ) (Cox and Chapman 2001).

Mean bubble size is assumed 2 mm in diameter. Also, this value is probably important from the viewpoint of velocity and turbulence field predictions, but it is critical in estimating

a local interfacial area  $a$  which is calculated using the following:

$$\alpha = 6 \times \frac{\alpha_{bub}}{d_{bub}} \quad (19)$$

Prediction of the value of  $k_L a$  can be done from the correlation given below.

$$K_L a = K_L \times a \quad (20)$$

## Results and discussion

Microorganisms are living creatures, sensitive to environmental conditions for their growth and survival and to continue their metabolism activities. Therefore, it is necessary to truly predict the impact of the shear caused by mixing rate, type of impeller and especially aeration intensity on those types of aerobic microorganisms.

CFD is a useful tool to get sufficient knowledge about the two major factors which affect the activity of aerobic microorganisms, namely, the oxygen mass transfer coefficient and shear rates on different positions of bioreactors. Cell growth rate has a direct relationship with oxygen mass transfer and on the other hand inversely effected by shear rate. Confirming of this claim from CFD modeling by experimental results for cell concentration during bioreaction process time are very useful. The optimized conditions can be predicted from CFD calculations when considered besides cell growth profiles.

A number of simulations for different operational conditions of aeration rate and impeller agitation speed are run for different types of impeller blade configurations by using the CFD code Fluent 6.2. For the grid independency issue, results from CFD calculations for energy dissipation ( $\epsilon$ ) were first tested with 678,453 number of relatively voluminous and then 815,694 moderate cells. Finally, the comparison of these converged results of the chosen mesh sizes with the much finer one with 1,004,945 number of cells confirms the mesh independency satisfaction with a slight difference of 0.7% in the maximum possible extent. Since there are limitations to report all of the contours of variables, the results are only illustrated for some of the conditions and the rest are summarized in plots. Figure 3 shows the essential features of the computational domain and the types of impeller used. The measurement probe positions are selected corresponding to the more notable points from the flow study viewpoint (Fig. 3). In order to justify impeller selection, four impellers of different types are used: a flat six blade standard Rushton, a half pipe circular six blade impeller, a pitched flat six blade impeller, and a LIGHTNIN-C 200 impeller, abbreviated as RT, HPC, P6B, and LIGHTNIN-C 200, respectively. Our focus on impeller selection is due to the fact that they create different fluid flow

patterns as they rotate. These flow patterns are the primary considerations and critical to achieve the desired result. The most common flow patterns in mixing are axial and radial. Axial mixing is important when addressing the most common challenges in the mixing of solid particle contained solutions. Also, the camber of the blade in LIGHTNIN-C 200 increases the efficiency of the impeller, reducing its power to pumping ratio. The most technical benefit of this type is the laminar flow created by the camber of this impeller. This camber reduces turbulence (shear) substantially, which is the reason for selecting this type for shear-sensitive applications.

Distribution of velocity magnitude is a very important factor in bioreactors, which shows how well the species are distributed in the vessel. The influence of operational conditions and geometrical parameters is predicted by the CFD model. Figure 4 depicts velocity profiles colored by velocity magnitude in the central axial cross section of the bioreactor in addition to volumetric values of velocity distribution for two conditions of without air sparging and with high aeration rate for all types of impellers used. According to Fig. 4, there is no stagnation zone by air sparging to the aqueous phase. An adequate mixing in several parts of the tank subjected to the acceptable distribution of velocity is good evidence to approve the claim for the satisfactory distribution of species. A complete homogenous system would maximize the surface area of contact between the cells and aqueous medium for better mass transfer. The column charts next to the velocity counters provide information for us to have a wider vision to assess the distribution intensity of species. Furthermore, this chart is able to provide us the prospective for the determination of the suitable flow pattern by correct selection of impeller type. As it is shown, the impellers produce the radial flow of fluid, except the last type, in which the generated flow turns out to be of downward axial type.

In the case of non-aeration condition, there are some stagnation points in several sections of the culture medium, and the columns show inadequate distributions, while as the sparging is performed, the columns are rather well-distributed in comparison to the mentioned condition. Wang et al. in their work have demonstrated that the larger velocity gradient distribution from gassing out may be beneficial for culture mixing and homogenization which placed emphasis on our results (Wang et al. 2010). By comparing the height of the velocity bars in the column charts, it is possible to evaluate the geometric parameters of the impellers on the distribution qualities of species for the stirred tank bioreactor.

The least amounts for the minimum ranges of velocity are more obvious in Fig. 4g, h. This amount is further diminished when the LIGHTNIN-C 200 type is used as the stirrer. Hence, it may be concluded that the stagnation zone decreases as the axial component of velocity predominates. This conclusion is in accordance with the work of Ibrahim et al. introducing the axially pumping stirrers as the best for solid suspension at

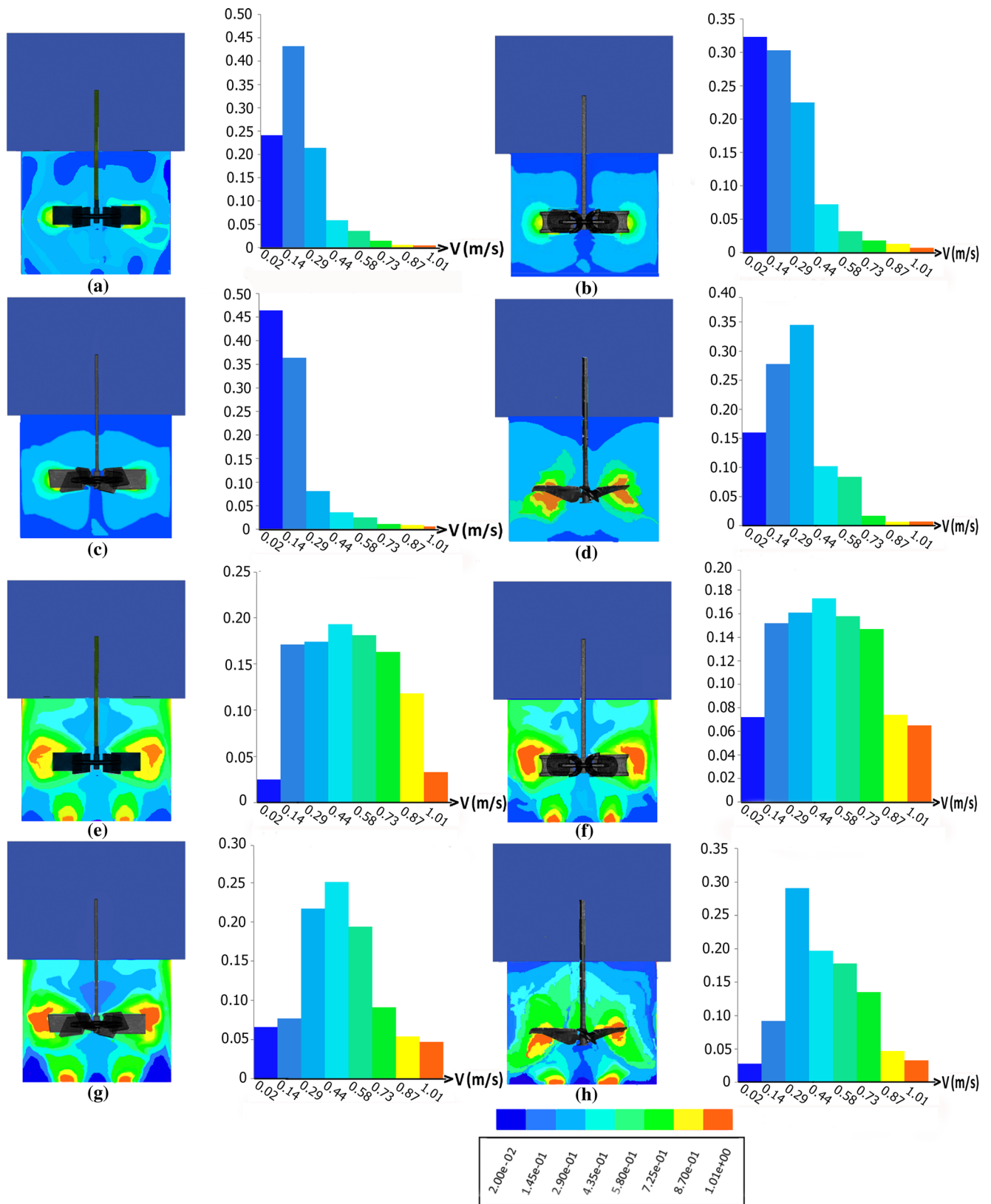


**Fig. 4** Velocity field and distribution for four types of impeller at 1000 rpm; 0 VVM-RT (a); 0 VVM-HPC (b); 0 VVM-P6B (c); 0 VVM-LIGHTNIN-C 200 (d); 0.2 VVM-RT (e); 0.2 VVM-HPC (f); 0.2VVM-P6B (g); 0.2VVM-LIGHTNIN-C 200 (h)



their optimal impeller-to-tank diameter ratio. The impellers used were axially downward pumping ones of different diameters, including a pitched six-blade mixed flow turbine. At their optimal D/T ratios, these impellers have been shown to be efficient for the suspension of denser particles (Ibrahim and Nienow 1996). This feature is considerably important when the performance of the conventional reactor is the objective of intention.

By elimination of the stagnation points in the reactor, the acceptable distribution of species that resulted from the potentially desirable degree of mass transfer would be achievable. Nevertheless, there are other limitations and problems confronted when we deal with biological systems. Shear stress is an important parameter in bioreactors which strongly influences the medium rheology and the microorganism morphology. Further, it is expected that the systems containing microorganisms are not able to tolerate more turbulences that can be generated when the mixing condition in bioreactor is too harsh. Therefore, the uniform distribution of velocity leads to better conditions from the viewpoint of shear analysis. This uniformity as well as oxygen delivery is undoubtedly an advantage for the growth of aerobic shear-sensitive microorganisms. Hence, a sensitive balance between mass transfer and shear stress has to be maintained by selecting a suitable and adequate operational condition, in which stirring rate is not that high to hurt the microorganism, but not that low to halt the rate of oxygen mass transfer. Therefore, it is strongly important to take the impeller type into account, which determines the flow regime and velocity distribution in the bioreactor. Figure 5 illustrates the experimental results related to the effect of impeller type selection on cell growth which is a fairly significant criterion to assess the performance of the bioreactor. The selected impeller should take the positive effect of oxygen transport to the greatest extent possible, and at the same time, undesirable effects of shear stress on microorganism morphology have to be reduced to the lowest level. According to the figure, it is obvious that the maximum cell growth is for the LIGHTNIN-C 200 type, which is in accordance with the concept of low shear producing design and downward directing forces which reduce the of possibly stagnation areas of the LIGHTNIN-C 200. At a recent time, Buffo et al. have quantified the average shear rate for a number of systems to find a combination that is the least harmful to the cell growth. The combination of EEDP and EEUP impeller types which are similar to LIGHTNIN-C 200 in topology was proved to be the most suitable case for the growth of the shear-sensitive aerobic microorganism, ensuring adequate mass transfer and minimizing cell damage (Buffo et al. 2016).

In non-aeration conditions, the influence of impeller blade topology is investigated as the only preferential factor. As can be seen in Fig. 4a–d, using the LIGHTNIN-C 200 type of impeller, the velocity distribution is better than the three other types. As shown in Fig. 4e–h, the LIGHTNIN-C 200 type

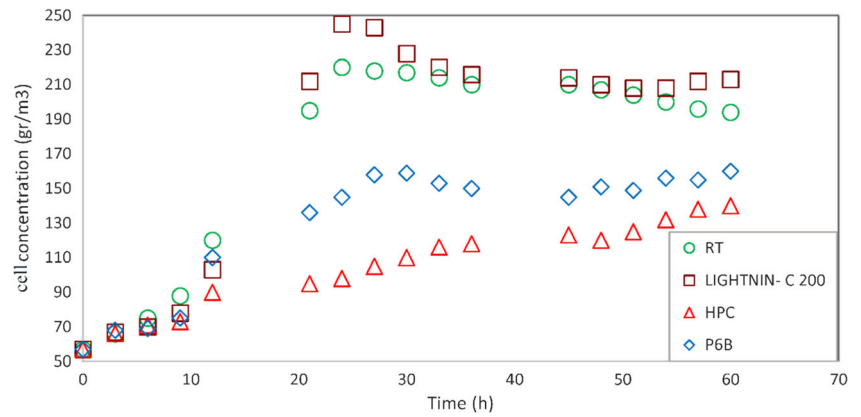
exhibits the least portion of maximum velocity in the distribution, which is good evidence to prove that the microorganism experiences less shear than the other types of impeller. On the other hand, the velocity distribution consists of a very low portion of the minimum velocity, which demonstrates that the mass transfer of oxygen from the bubble to the cell medium is not negatively affected when compared to the other types. Therefore, the maximum influence of the mass transfer process on the phenol biodegradation is observed when the LIGHTNIN-C 200 type is used. It can be concluded that utilization of the mentioned type by itself could lead to promising results from the shear analysis perspective. In this regard, aeration is an inevitable factor when it comes to aerobic microorganisms presented in the bioreaction medium. Now, the results obtained for the velocity profile in the case of aeration with the intensity of 0.2 volume of air per volume of medium per minute (VVM) can be discussed and compared with the corresponding column charts. Generally, the highest shear stress occurs in the locations where velocity increases intensively (Kaya et al. 2014). The effect of different impeller configurations on the contribution of aeration to velocity distribution is based on the different flow patterns developed by the type of impellers, as described in Fig. 4e–h. As far as the height of the maximum velocity bar is lower, the damages caused by shear stress are reduced. On the other hand, given that the definition of shear rate is based on the local velocity variations, the monotonous columns can be of vital importance as well as the height of the very first and last columns are in the assessments. As it is observed, RT and HPC impellers show more stagnation zones, but with less difference in the column height distributions. However, as the flow pattern turns to axial flow from the radial using P6B and LIGHTNIN-C 200, less stagnation points and more decreasing trends are observed at higher velocities. Moreover, by comparing the two latest impeller types, LIGHTNIN-C 200 comprises a smaller area of both maximum and minimum values of the velocity, which is a good evidence for LIGHTNIN-C 200 to be considered as the most promising option in terms of hydrodynamic characteristics.

The value of shear rate is measured as a function of agitation speed for the most four prominent sections including sparger domain, impeller region, top territory, and baffle nearby, respectively (Fig. 3).

Figure 6 simultaneously illustrates the results obtained by CFD calculations along with the experimental measurements by limiting current electro-diffusion method for the four types of impellers.

As commented above, the presented calculations refer to the local shear rate of the liquid and do not take into account velocity fluctuations generated from internal coordinates such as bubble size distribution. The greatest value of shear rate occurs over a narrow region in the vicinity of the rotating impeller blades. As can be seen, this trend is the same for all

**Fig. 5** Comparison of the measured cell growth in the cell medium for different impeller configuration



types of the impellers. The influence of the gas sparger on the generated shear stress is found to be obvious as point 1 in Fig. 3 in the very nearness of the sparger orifices, which allocated the second highest value of all to itself. The reason for the sharp reduction of shear around the surface level is perfectly understandable. The above-discussed behavior has the same trend for all types of impellers used (Fig. 6). The results from CFD shear analysis are confirmed by the experimental measurements using electro-diffusion method with good agreement. The separate cases of the four types of impeller are simulated and post-processed by CFD and two types of impellers corresponding to complete radial flow (RT impeller) and complete axial flow (LIGHTNIN-C 200) are analyzed. Figure 7 reveals a similar trend in terms of shear rate iso-surfaces and visualizes the results reported in Fig. 6 in an example condition of 300 rpm 0.2 VVM for five selected shear rates.

Shear rate profile in the radial direction at the aeration rate of 0.2 VVM and agitation speed of 100 rpm is shown in Fig. 8. The data averaging is justified for two reasons: to average the velocity gradient components dominating in various measurement positions and to minimize the flow fluctuation effect on the time course of the limiting current. From the mentioned diagram, it is clear that as much as the flow pattern goes to the axial type from the radial, the shear value takes a more monotonous state. From Fig. 4e–h, when aeration comes along with agitation in the bioreactor, the main direction of the flow is upward which is dominated by the direction of sparged oxygen bubbles. The rule of impeller is to distribute the flow in the radial direction to cover all the points of the medium. However, there is still some stagnation points in the lower edges of the bioreactor, which needs the flow to turn over to this area. Downward axial mixing by the LIGHTNIN-C 200 impeller eliminates this problem. According to Fig. 8, lower

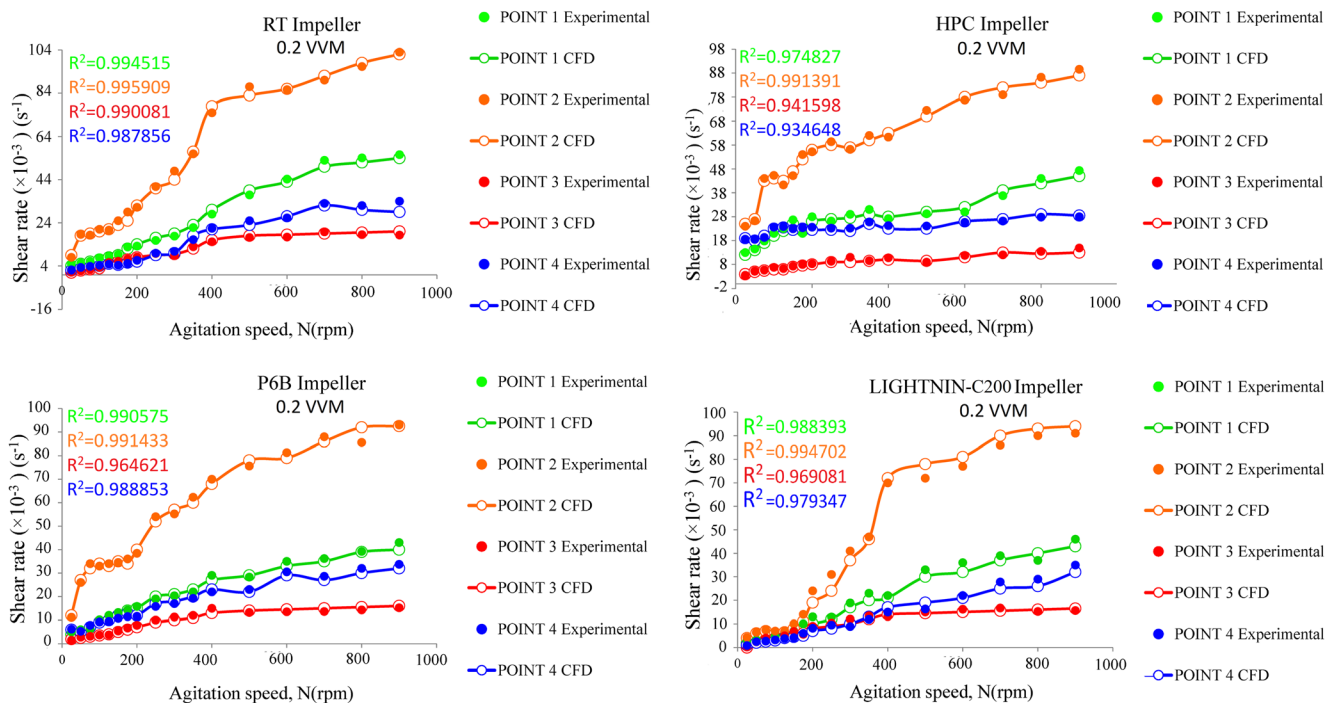


**Fig. 6** Shear rate for four types of impellers in four points of the bioreactor as a function of agitation velocity at 0.2 VVM

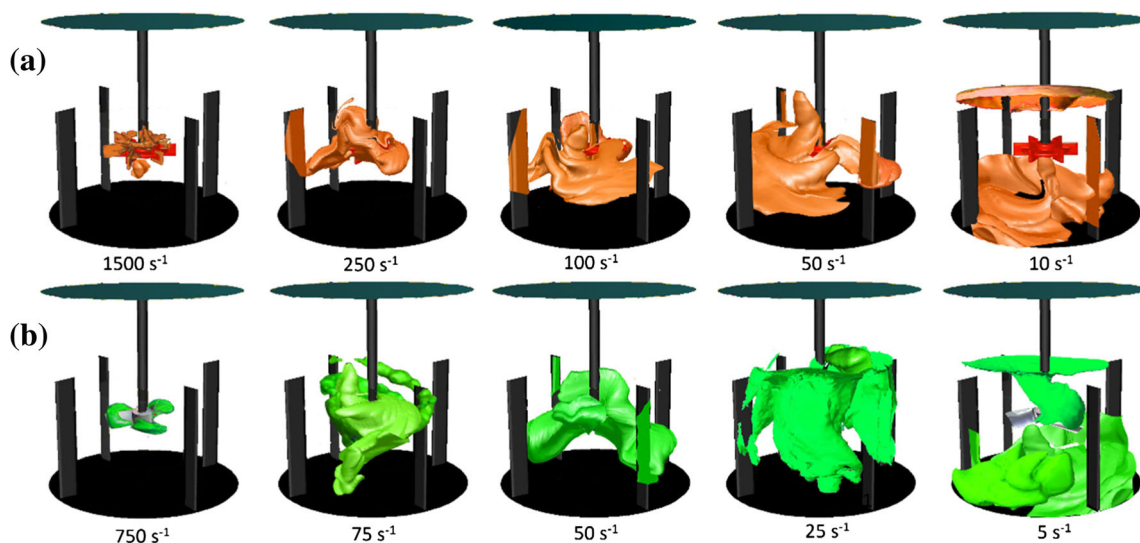


**Fig. 7** Iso-zones corresponding to different strain levels for radial and axial distributions; RT impeller (a); LIGHTNIN-C 200 impeller (b)

values of the shear rate can be seen for the LIGHTNIN-C 200 type. The dependence of the volumetric mass transfer coefficient on aeration rate is shown in Fig. 9. This figure simultaneously illustrates the results obtained by CFD calculations along with the experimental measurements. It can be observed that, with an increase in the rate of aeration, the magnitude of  $k_{La}$  increases for all types of impellers without exception. The slope of the curves decreases at higher gas flow rates by getting closer to the saturation of the dissolved oxygen concentration. The value of  $k_{La}$  is obtained for different gas aeration rates, all types of impellers depicted in Fig. 3, and in a wide range of impeller rotational speed from 0 to 1000 rpm. As can be seen, P6B provides the best oxygen mass transfer. However, other types represent the adequate amount of  $k_{La}$ . Recently, in a similar work by Scargiali et al., the influence of impeller geometry on oxygen mass transfer performance was investigated for an un-baffled system. Their experimental results showed that a simple pitched blade turbine type among the impeller geometries was found to provide the most interesting oxygen transfer performance and can therefore be

regarded as a particularly suitable impeller for shear-sensitive cultures (Scargiali et al. 2014).

The results include both CFD and experimental data. All the results are collected in order to evaluate data confirmation in Fig. 10. The DO measurements are all in agreement with each other and, thereby,  $k_{La}$  analysis is based on the average value of  $k_{La}$  from DO values in the reactor. The paper compares globally averaged  $k_{La}$  (spatially averaged value of the four retrospectively selected points) from experiments with the integration results of all CFD local  $k_{La}$  values (globally averaged  $k_{La}$ ) in Figs. 9 and 10. To be more precise, according to Fig. 10, the experimental  $k_{La}$  turns out to lie within the experimentally measured values. The residual sum of squares between CFD and experimental values of  $k_{La}$  in the parity diagram (Fig. 10) shows the simulation validity for the Eulerian model. The deviation from the  $k_{La}$  value was low in the 0.15 VVM (around 2.65%) but higher in the 0.2 and 0.3 VVM sparging rates (8.9 and 9.2%, respectively). This can be explained by the error magnitude of presumably bubble volume changes that occurred by bubble interactions in the

**Fig. 8** CFD profiles for shear rate corresponding to different types of impellers at 0.2VVM and 100 rpm

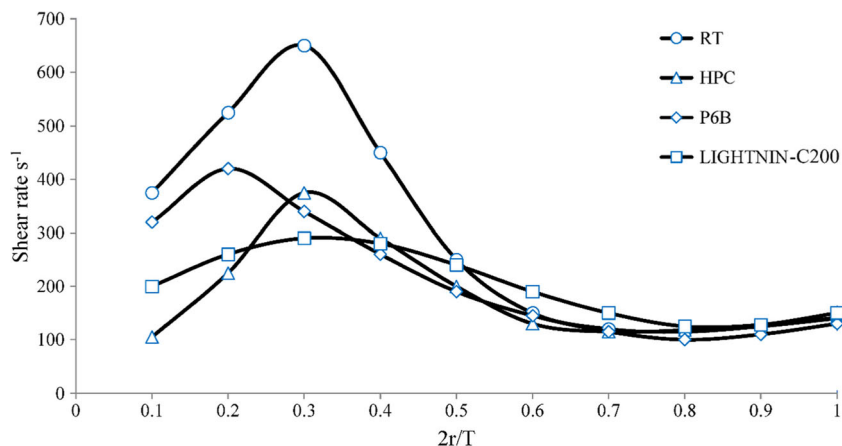
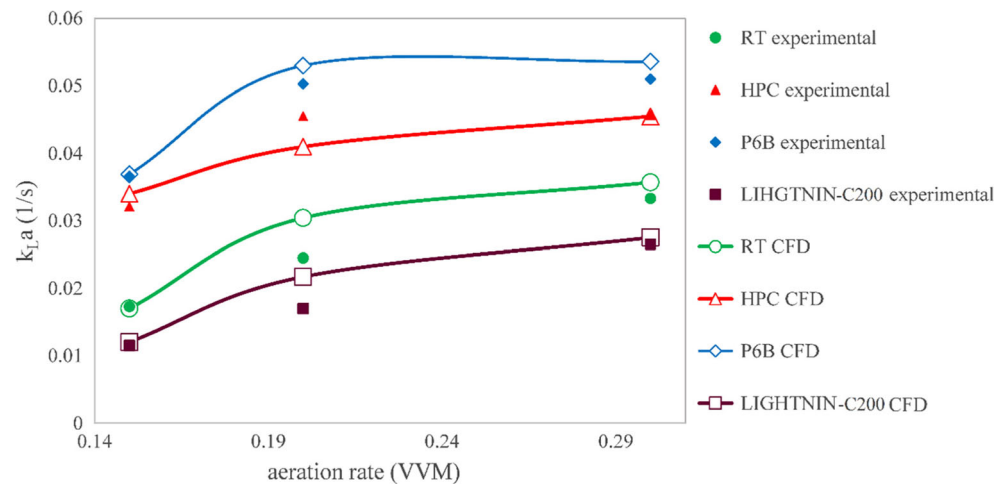


**Fig. 9** CFD calculation and experimentally measured volumetric mass transfer coefficient as a function of sparging gas velocity at 100 rpm



up-moving process of oxygen transfer. The CFD average volumetric values reported in Fig. 10 are obtained from the integration of the local values in the reactor domain. The measured cell concentration growth in Fig. 11 approves the contributing effect of aeration rate on the proper execution of oxygen mass transfer to get contact with the microorganism surface. The same trend has been reported in the work of Scargiali et al. (2014). The reverse trend is observed by increasing the agitation speed in Fig. 12. As can be seen, the impeller rotational speed has a reverse correlation with the cell growth, which can be attributed to the generated harsh shear conditions, which threatens the life of microorganisms. In agreement with the present work, the same trend has also been demonstrated in a diagram of the average shear rate as a function of operating condition by Buffo et al. (2016). Therefore, the point of this paper is that the CFD model is capable to predict the local quantities which could not all be measured. Although the ability to predict the volumetric  $k_La$  which is integrated from the calculated local values in agreement with an experimental measurement does not represent much of an advance, but is the new

knowledge that opens a new window to clearly estimate mass transfer coefficient from CFD. The simulation results are comparable with the volumetric mass transfer  $k_La$  from the gassing out experiments. This can approve our model for further applications when there are some limitations in operating experimental measurements. The CFD-predicted local value of  $k_La$  is of vital importance once we face some practical limitations in experiments. One of the limitations is to conduct experimental measurements where there is no access to insert the probe (e.g., in the impeller region) to determine shear rate values. Another limitation is attributed to the fermenters which are operated at high density and in the presence of high levels of complex particles that restricts the available measurement techniques. This limitation in the complex media is typically due to microbial growth on probe surfaces. Such growth leads to substantial calibration and linearity problems. Alternately, CFD simulation based on the validated models is capable to provide the necessary information of the total mass of cells and give an accurate description of shear rate conditions for the microorganisms to grow and survive.

**Fig. 10** Comparison between calculated  $k_La$  and experimental  $k_La$  for impellers of RT, HPC, P6B, and LIGHTNIN-C 200 in three aeration rates of 0.15, 0.2, and 0.3 VVM and from 100 to 1000 rpm

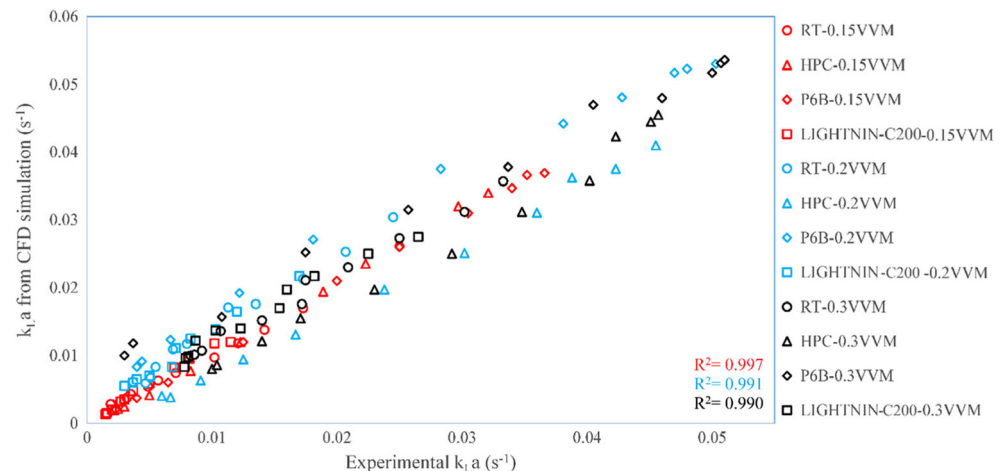
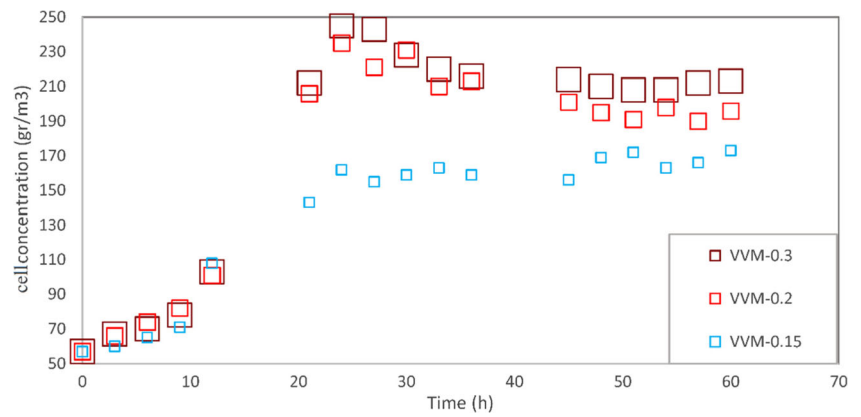


**Fig. 11** Experimental cell growth vs submerged aeration rate for the LIGHTNIN-C 200 geometry



**Conclusions**

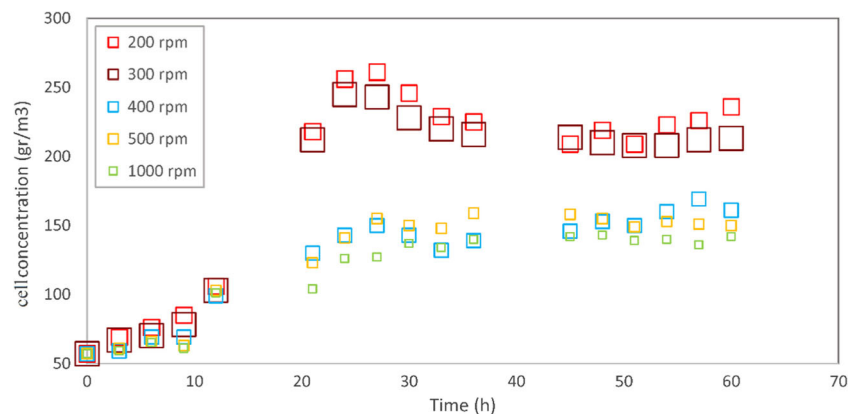
This paper improved an aerated stirred bioreactor design and studied the effects of impeller type on velocity distribution, shear rate, and oxygen mass transfer to optimize cell growth. The rate of shear stress in different sections of the bioreactor and the overall oxygen mass transfer coefficient were calculated and compared with the microorganisms’ growth rate from the experiments. The measured results of cell growth could be attributed to two main factors: (1) oxygen mass transfer coefficient representing how much oxygen was supplied to maintain the metabolic activity of microorganisms and (2) shear stress generated from different operation conditions and affecting microorganism morphology.

Evaluation of the experimentally compared CFD calculations showed that more axial flow patterns led to minimum stagnation zones. Therefore, LIGHTNIN-C 200 represented more enhanced results by reflecting the flow to the bottom corner stagnation areas of the bioreactor compared to partially axial (P6B) and radial (RT and HPC) patterns. Although LIGHTNIN-C 200 took the back seat for high viscosity flow-controlled applications, it could be suitable for low- and medium-viscosity fluids as in our case. For the low-viscosity cases, gas dispersion typically

requires a high power input per unit volume. Nevertheless, due to the sensitivity of the microorganism for higher values of parallel acting forces between the sliding layers coming from velocity variation which leads to shear stress, the axial type of LIGHTNIN-C 200 was selected for shear-sensitive applications. It is obvious that, with an increase in the aeration flow rate,  $k_La$  values increased, which is why cell growth rate increased by increasing aeration. Moreover, the created stagnation zones due to improper mixing process in the vessel led to poor oxygen mass transfer. By contrast, cell rupture was more prevalent in the positions where the higher values of velocity led to intolerable shear stress on the cell surfaces. Hence, it would be beneficial to use LIGHTNIN-C 200, since the distribution of velocity shows more uniformity.

$\alpha$ , volume fraction;  $\varepsilon$ , turbulent dissipation energy ( $m^2/s^3$ );  $\mu$ , viscosity ( $kg/ms$ );  $\rho$ , density ( $kg/m^3$ );  $\tau$ , shear stress ( $kg/ms^2$ );  $\bar{\tau}_{eff}$ , effective viscous stress tensor ( $kg/ms^2$ );  $\mu$ , laminar molecular viscosity( $kg/ms$ );  $\mu_{turb}$  turbulent viscosity( $kg/ms$ );  $\gamma$ , shear strain rate (1/s);  $\alpha$ , interfacial area per unit volume ( $1/m$ );  $C_b$ , bulk concentration of the ions ( $mole/m^3$ );  $C_D$ , drag coefficient;  $C_L$ , oxygen concentration ( $mole/m^3$ );  $D$ , diffusivity ( $m^2/s$ );  $d_e$ , circular microelectrode diameter (m);  $D_{eff}$  diffusion coefficient of active ions in the solution( $m^2/s$ );  $d_v$ , Droplet diameter (m); F, Faraday constant (s A / mol);  $F_C$ ,

**Fig. 12** experimental cell growth vs rotational speed for the LIGHTNIN-C 200 geometry



centrifugal force ( $\text{N/m}^3$ );  $F_i$ , phase interaction force ( $\text{N/m}^3$ );  $\bar{\Gamma}$ , unit tensor;  $I_d$ , local diffusion limiting current;  $K_L$ , mass transfer coefficient ( $\text{m/h}$ );  $K_L a$ , volumetric mass transfer coefficient ( $1/\text{h}$ );  $N$ , frequency of rotation (rpm, r/min);  $n_e$ , number of exchanged electrons;  $P$ , pressure (Pa);  $U$ , Reynolds-averaged velocity (m/s)

### Compliance with ethical standards

**Conflict of interest** We wish to confirm that there are no known conflicts of interest associated with this publication and there has been no significant financial support for this work that could have influenced its outcome. We confirm that the manuscript has been read and approved by all named authors and that there are no other persons who satisfied the criteria for authorship but are not listed. We further confirm that the order of authors listed in the manuscript has been approved by all of us. We understand that the Corresponding Author is the sole contact for the Editorial process (including Editorial Manager and direct communications with the office). He is responsible for communicating with the other authors about progress, submissions of revisions, and final approval of proofs. We confirm that we have provided a current, correct email address which is accessible by the Corresponding Author and which has been configured to accept email from hamed.moradkhani@yahoo.com.

### References

- Ahmadi G, Ma D (1990) A thermodynamical formulation for dispersed multiphase turbulent flows—I: basic theory. *Int J Multiphase Flow* 16:323–340
- Anderson JD, Wendt J (1995) Computational fluid dynamics. In: Anderson JD (ed) *Governing equations of fluid dynamics* 3rd edn. Springer, Berlin, pp 34–40
- Bakker A (1992) Hydrodynamics of stirred gas-liquid dispersion. Ph. D. thesis, Delf University of Technology, The Netherlands, pp 86–88
- Bakker A, Akker HA (1994) A computational model for the gas-liquid flow in stirred reactors. *Chem Eng Res Des* 72:594–606
- Bartrand TA, Farouk B, Haas CN (2009) Countercurrent gas/liquid flow and mixing: implications for water disinfection. *Int J Multiphase Flow* 35:171–184
- Buffo M, Corrêa L, Esperança M, Cruz A, Farinas C, Badino A (2016) Influence of dual-impeller type and configuration on oxygen transfer, power consumption, and shear rate in a stirred tank bioreactor. *Biochem Eng J* 114:130–139
- Contreras A, García F, Molina E, Merchuk JC (1999) Influence of sparger on energy dissipation, shear rate, and mass transfer to sea water in a concentric-tube airlift bioreactor. *Enzym Microb Technol* 25:820–830
- Cox KR, Chapman WG (2001) The properties of gases and liquids, by Bruce E. Poling (University of Toledo), John M. Prausnitz (University of California at Berkeley), and John P. O'Connell (University of Virginia). McGraw-hill: New York. 2001. 768 pp. \$115.00. ISBN 0-07-011682-2. ACS Publications
- Dey A, Bhunia B, Dutta S (2016) Studies on the effect of agitation and aeration for the improved protease production by bacillus licheniformis NCIM-2042. *Mater Today Proc* 3:3444–3449
- Douhal M (1977) Mechanism of disintegration of biological cells in ultrasonic cavitation. *Biotechnol Bioeng* 19:649–660
- Douhal M, Hammond T, Brookman J (1975) A hydrodynamic mechanism for the disintegration of *Saccharomyces cerevisiae* in an industrial homogenizer. *Biotechnol Bioeng* 17:845–858
- Ferreira A, Pereira G, Teixeira J, Rocha F (2012) Statistical tool combined with image analysis to characterize hydrodynamics and mass transfer in a bubble column. *Chem Eng J* 180:216–228
- Fluent Inc (2006) *Fluent 6.3 user's guide*. Canonsburg, Pennsylvania, United States
- Franz K, Börner T, Kantorek HJ, Buchholz R (1984) Strömungsstruktur in blasensäulen. *Chem Ing Tech* 56:154–155
- Gogate PR, Pandit AB (1999) Survey of measurement techniques for gas-liquid mass transfer coefficient in bioreactors. *Biochem Eng J* 4:7–15
- Ibrahim S, Nienow A (1996) Particle Suspension in the Turbulent Regime-The Effect of Impeller Type and Impeller/Vessel Configuration. *Chem Eng Res Des* 74:679–688
- Ishii M, Zuber N (1979) Drag coefficient and relative velocity in bubbly, droplet or particulate flows. *AIChE J* 25:843–855
- Juang R-S, Kao H-C, Tseng K-J (2010) Kinetics of phenol removal from saline solutions by solvent extraction coupled with degradation in a two-phase partitioning bioreactor. *Sep Purif Technol* 11:285–292
- Juang R-S, Kao H-C, Zhang Z (2012) A simplified dynamic model for the removal of toxic organics in a two-phase partitioning bioreactor. *Sep Purif Technol* 12:213–220
- Kawase Y, Halard B, Moo-Young M (1992) Liquid-phase mass transfer coefficients in bioreactors. *Biotechnol Bioeng* 39:1133–1140
- Kaya R, Deveci G, Turken T, Sengur R, Guclu S, Koseoglu-Imer DY, Koyuncu I (2014) Analysis of wall shear stress on the outside-in type hollow fiber membrane modules by CFD simulation. *Desalination* 351:109–119
- Kohles SS, Nève N, Zimmerman JD, Trethewey DC (2009) Mechanical stress analysis of microfluidic environments designed for isolated biological cell investigations. *J Biomech Eng* 131:121006
- Laakkonen M, Moilanen P, Alopaeus V, Aittamaa J (2007) Modelling local gas-liquid mass transfer in agitated vessels. *Chem Eng Res Des* 85:665–675
- Labik L, Moucha T, Petříček R, Rejl J, Valenz L, Haidl J (2017) Volumetric mass transfer coefficient in viscous liquid in mechanically agitated fermenters. Measurement and correlation. *Chem Eng Sci*. doi:10.1016/j.ces.2017.04.006
- Lamont JC, Scott D (1970) An eddy cell model of mass transfer into the surface of a turbulent liquid. *AIChE J* 16:513–519
- Laurenzi F, Coroneo M, Montante G, Paglianti A, Magelli F (2009) Experimental and computational analysis of immiscible liquid-liquid dispersions in stirred vessels. *Chem Eng Res Des* 87:507–514
- Mallevre F, Fernandes TF, Aspray TJ (2016) *Pseudomonas putida* biofilm dynamics following a single pulse of silver nanoparticles. *Chemosphere* 153:356–364
- Melgarejo-Torres R, Torres-Martínez D, Gutiérrez-Rojas M, de Jesús AG, Lye G, Huerta-Ochoa S (2011) Regime analysis of a Baeyer-Villiger bioconversion in a three-phase (air-water-ionic liquid) stirred tank bioreactor. *Biochem Eng J* 58:87–95
- Menzel T, Kantorek HJ, Franz K, Buchholz R, Onken U (1985) Zur Strömungsstruktur in Airlift-Schlaufenreaktoren. *Chem Ing Tech* 57:139–141
- Michelin M, de Oliveira Mota AM, de Moraes MLT, da Silva DP, Vicente AA, Teixeira JA (2013) Influence of volumetric oxygen transfer coefficient ( $k_L a$ ) on xylanases batch production by *Aspergillus niger* van Tieghem in stirred tank and internal-loop airlift bioreactors. *Biochem Eng J* 80:19–26
- Moradkhani H, Kouchehbagh NA, Izadkhan M-S (2016) Experimental and CFD-PBM approach coupled with a simplified dynamic analysis of mass transfer in phenol biodegradation in a three phase system of an aerated two-phase partitioning bioreactor for environmental applications. *Heat Mass Transfer* 53:1073. doi:10.1007/s00231-016-1876-4
- Moutafchieva D, Popova D, Dimitrova M, Tchaoushev S (2013) Experimental determination of the volumetric mass transfer coefficient. *J Chem Technol Metall* 48:351–356

- Paul EL, Atiemo-Obeng VA, Kresta SM (2004) Handbook of industrial mixing: science and practice. In: Kresta SM (ed) *Turbulence in Mixing Applications*. Wiley-Interscience, New York, pp 63
- Pauli J, Menzel T, Onken U (1989) Directional specific shear-rate measurements in gas-liquid two-phase flow. *Chem Eng Technol* 12:374–378
- Puthli MS, Rathod VK, Pandit AB (2005) Gas-liquid mass transfer studies with triple impeller system on a laboratory scale bioreactor. *Biochem Eng J* 23:25–30
- Qi N, Zhang H, Zhang K, Xu G, Yang Y (2013) CFD simulation of particle suspension in a stirred tank. *Particuology* 11:317–326
- Ramezani M, Kong B, Gao X, Olsen MG, Vigil RD (2015) Experimental measurement of oxygen mass transfer and bubble size distribution in an air-water multiphase Taylor-Couette vortex bioreactor. *Chem Eng J* 279:286–296
- Scargiali F, Busciglio A, Grisafi F, Brucato A (2014) Mass transfer and hydrodynamic characteristics of unbaffled stirred bio-reactors: influence of impeller design. *Biochem Eng J* 82:41–47
- Sungkorn R, Derksen J, Khinast J (2012) Modeling of aerated stirred tanks with shear-thinning power law liquids. *Int J Heat Fluid Flow* 36:153–166
- Trad Z, Vial C, Fontaine J-P, Larroche C (2017) Mixing and liquid-to-gas mass transfer under digester operating conditions. *Chem Eng Sci*. doi:10.1016/j.ces.2017.01.056
- Wang X, Ding J, Guo W-Q, Ren N-Q (2010) A hydrodynamics-reaction kinetics coupled model for evaluating bioreactors derived from CFD simulation. *Bioresour Technol* 101:9749–9757
- Wase D, McManamey WJ, Raymahasay S, Vaid AK (1985) Comparisons between cellulase production by *Aspergillus fumigatus* in agitated vessels and in an air-lift fermentor. *Biotechnol Bioeng* 27:1166–1172
- Wilson ZD, Kohles SS (2010) Two-dimensional modeling of nanomechanical strains in healthy and diseased single-cells during microfluidic stress applications. *J Nanotechnol Eng Med* 1:021005
- Zhao Y, Wu J, Yuan X, Zhu W, Wang X, Cheng X, Cui Z (2017) The effect of mixing intensity on the performance and microbial dynamics of a single vertical reactor integrating acidogenic and methanogenic phases in lignocellulosic biomass digestion. *Bioresour Technol* 238:542–551
- Zokaei-Kadijani S, Safdari J, Mousavian M, Rashidi A (2013) Study of oxygen mass transfer coefficient and oxygen uptake rate in a stirred tank reactor for uranium ore bioleaching. *Ann Nucl Energy* 53:280–287